This article has been accepted for publication in a future issue of this journal, but has not been fully edited. Content may change prior to final publication. Citation information: DOI 10.1109/LPT.2019.2896560, IEEE Photonics Technology Letters

Grating Coupled Silicon-on-Sapphire Polarization Rotator Operating at Mid-Infrared Wavelengths

Ali Rostamian, *Member, IEEE*, Joel Guo, Swapnajit Chakravarty, *Senior Member, IEEE*, Hai Yan, Chi-Jui Chung, Elham Heidari, and Ray T. Chen, *Fellow, IEEE*

***Abstract*— We provide an experimental demonstration of mid-infrared polarization rotators built on a silicon-on-sapphire platform at the mid-infrared (mid-IR) wavelength of 4.55μm to enable integration of quantum cascade lasers (QCLs) and detectors with slotted photonic crystal waveguide (PCW) gas sensors for on-chip optical spectroscopy applications. Polarization rotators are essential to convert the preferentially transverse magnetic (TM) polarized light from a QCL to transverse electric (TE) polarization to interface with the preferential TE-guiding slotted PCW sensors The polarization rotator consists of an adiabatic tapered mode converter followed by a phase shifter and a multimode interferometer that effectively transfers energy from an input fundamental TM_{00} polarization to first-order TE_{10} polarization that is then converted to the fundamental TE_{00} mode. Polarization selective sub-wavelength grating couplers are designed and fabricated to effectively couple TE or TM polarizations at the designed wavelengths into and out of the polarization rotator device for efficient device characterization. TM_{00} to TE_{10} conversion efficiency of 100% is simulated. Fabrication tolerances in the phase shifter result in an experimental 80:20 splitting ratio of the measured output TE_{00} polarized light between two output arms.**

***Index Terms*—Silicon photonics, optical polarization, polarization rotation, mid-infrared, waveguide couplers, gratings**

I. Introduction

POTENTIAL applications of silicon photonics in the mid-infrared (MIR) regime including gas sensing, bio-agent and medical sensing, thermal imaging, astronomy, free-space communication and environmental monitoring has drawn increasing attention in recent years [1-5]. Owing to the unique molecular vibration signature and large absorption cross-section of the compounds and gases in the mid-IR wavelengths, spectroscopy in this regime is considered as a promising technique in sensing applications [6]. Commercial infrared spectroscopy systems have bulky and expensive optical components and are not suitable for low size, weight and power (SWaP) applications such as the devices used inside airborne platforms and space-crafts [7].

Slow Light effect and enhanced optical mode overlap with the analyte in photonic crystal waveguides (PCWs) has made these structures an ideal platform for on-chip mid-IR absorption sensors. we have demonstrated sensors based on holey and slotted photonic crystal waveguides (HPCWs) that have shown feasibility of the detection of sub-100 parts per billion (ppb) concentration of greenhouse gases such as carbon monoxide [8], volatile organic compounds (VOCs) such as xylene and trichloroethylene [9,10] and other analytes [6]. The absorption principle is based on increasing interaction time between propagating wave and analyte of interest by slowdown of light in the waveguide and also enhancement of the optical mode overlap integral with the analyte at the middle of the PCW. Availability of high-power, inexpensive and reliable quantum cascade lasers (QCLs) and high Mid-IR bandwidth quantum cascade detectors (QCDs) has paved the way for building a feasible optical setup in the mid-IR [11] but in order to realize a low SWaP device and make an on-chip spectrometer, the PCW, QCL and QCD need to be monolithically integrated. The emission from the QCL is transverse magnetic (TM) polarized. 2-D slotted PCWs have photonic band gaps (PBGs) for transverse electric (TE) polarized propagating light only. Hence, a polarization rotator is required to rotate TM-polarized light from QCL to TE-polarized light in the slotted PCW. Various polarization rotators have been experimentally demonstrated at telecom wavelengths [12-15] using single-step and multi-step lithography processes. Multi-step lithography processes in particular require fine alignment tolerances between successive fabrication layers. In this paper, we design, fabricate and experimentally demonstrate an efficient polarization rotator in silicon-on-sapphire (SoS) at λ=4.55μm which can be fabricated in one lithography step. SoS is chosen due to transparency of sapphire cladding till l~5μm that enables low waveguide propagation loss [19].

II. Device Design

The schematic of the polarization rotator is shown in Fig. 1(a). The cross-sectional geometry of the silicon waveguide is

This work was supported in part by National Science Foundation (NSF) under Contract 1711824 and in part by the NASA SBIR Program under Grant NNX17CA44P.

A. Rostamian, J. Guo, H. Yan, C.-J. Chung, E. Heidari, and R. T. Chen are with the Microelectronic Research Center, Department of Electrical and Computer Engineering, University of Texas at Austin, Austin, TX 78758 USA (e-mail: ali.rostamian@utexas.edu; joel.guo@utexas.edu; hai.yan@utexas.edu; cjchung@utexas.edu; e.heidari@utexas.edu; chenrt@austin.utexas.edu).

S. Chakravarty is with Omega Optics Inc., Austin, TX 78757 USA (e-mail: swapnajit.chakravarty@omegaoptics.com).

This article has been accepted for publication in a future issue of this journal, but has not been fully edited. Content may change prior to final publication. Citation information: DOI 10.1109/LPT.2019.2896560, IEEE Photonics Technology Letters

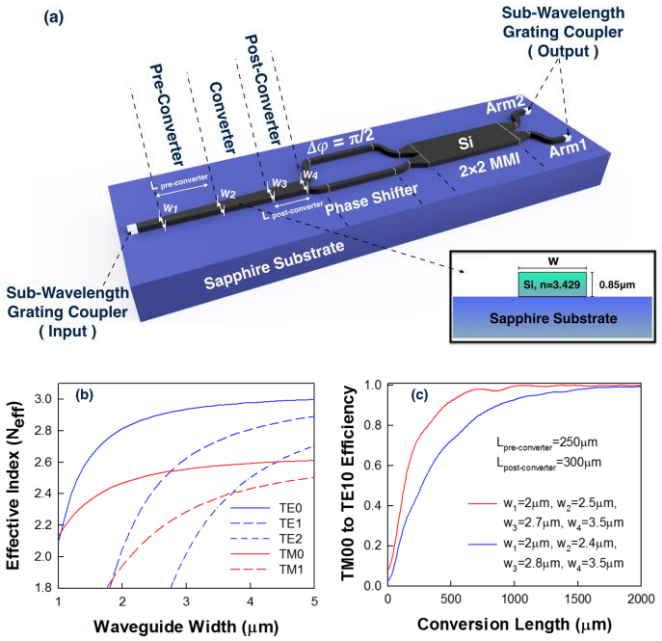

Fig. 1. (a) Schematic of a polarization rotator splitter, similar to the design in Ref. 13. inset is the cross-section geometry of the silicon waveguide, (b) Effective Index versus width (w) of waveguide of the propagating waveguide modes simulated by finite-element modeling (FEM) for the waveguide structure in the inset of 1(a), (c) TM_{00} to TE_{10} conversion efficiency at λ=4.55μm versus length of the converter section for Device1(red curve) : pre-converter width changes from 2μm to 2.5μm over 250μm, converter width changes from 2.5μm to 2.7μm and post-converter width changes from 2.7μm to 3.5μm over 300μm and Device2 (Blue curve) : pre-converter width changes from 2μm to 2.4μm over 250μm, converter width changes from 2.4μm to 2.8μm and post-converter width changes from 2.8μm to 3.5μm over 300μm.

shown in the inset of Fig 1(a). The device consists of a TM_{00} to TE_{10} mode converter, followed by a phase shifter and a 2×2 MMI. Light is first coupled from a single mode mid-IR fiber (IRFlex) into an input single mode waveguide of width w~2μm, through a polarization selective sub-wavelength grating (SWG) coupler. As shown in Fig. 1(a), the input coupled light passes through an adiabatically tapered mode converter which is divided into pre-converter, converter and post-converter sections. Fig. 1(b) plots the effective index (Neff) versus waveguide width (w) for the structure in the inset of Fig. 1(a) at the wavelength of 4.55μm. It can be observed in Fig. 1(b) that TM_{00} to TE_{10} mode conversion occurs at a waveguide width of w~2.55μm. The pre-converter (post-converter) sections of the device are short tapers 250μm (300μm) long where the width increases from 2μm to 2.4μm, and from 2.7μm to 3.5μm respectively. The central converter section is adiabatically tapered from 2.4μm to 2.8μm over a 2mm length to achieve 98% conversion efficiency from TM_{00} to TE_{10} polarization, as shown in Fig. 1(c). Fig. 1(c) also shows that a more aggressive design with the converter section tapered from 2.5μm to 2.7μm can achieve ~98% conversion efficiency from TM_{00} to TE_{10} over a length of 1mm thereby resulting in a more compact device. In this demonstration, we fabricated the 2mm long converter tapering from 2.4μm to

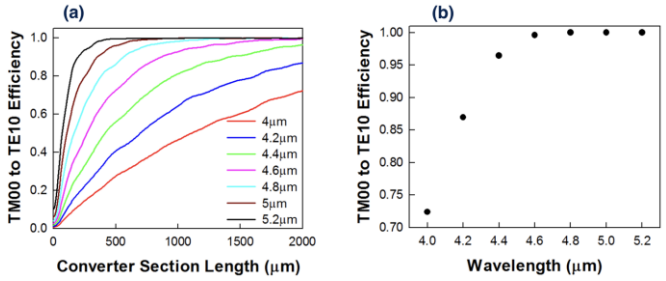

Fig. 2. Eigenmode expansion simulation for conversion efficiency of TM_{00} to TE_{10} as a function of (a) the length of the converter section for different wavelengths and (b) wavelength for 2mm converter length for dimensions given by blue curve in Fig. 1(c).

2.8μm, to account for potential fabrication imperfections of the waveguide widths.

The converted TE_{10} wave then splits into two 180 -degree phase shifted TE_{00} beams propagating in the single mode waveguide arms of a phase shifter. The post-converter ending width was chosen as 3.5μm to effectively split into two single mode 1.75μm wide TE_{00} guiding waveguides, as simulated in Fig. 1(b). A waveguide phase shifter is designed as a Bezier curve, to introduce an additional $\pi/2$ phase difference between the two input arms of the 2×2 MMI of dimensions 10μm by 117μm. With the chosen parameters, an input TM_{00} mode at the input grating coupler is rotated to TE_{00} and output to the upper arm (designated arm 2 in Fig. 1(a)). The fraction of energy in TM_{00} that is not converted to TE_{10} (and thus TE_{00}) is routed to the lower arm 1. The phase shifter dimensions are critical since deviations from the ideal $\pi/2$ phase difference between the two phase shifter arms affects the TE_{00} splitting ratio between the two output arms for both input polarization cases. For our selected design parameters, the output from arm1 is negligible. On the contrary, an incoming TE_{00} input would be preserved in the converter section and finally routed to the lower arm 1 with negligible signal in the upper arm 2. Therefore, in principle, our device behaves as a polarization rotator-splitter and delivers a TE_{00} output from either arm1 or arm2 depending on the input polarization. The output from the device is collected by a mid-IR fiber via output SWG couplers and measured by a detector. Fig. 2(a) and 2(b) show eigenmode expansion (EME) simulation for conversion efficiency of TM_{00} to TE_{10} as a function of the length of the converter section (for different wavelengths) and wavelength respectively, for device dimensions given by the blue curve in Fig. 1(c). Fig. 3 illustrates 3D finite-difference-time-domain

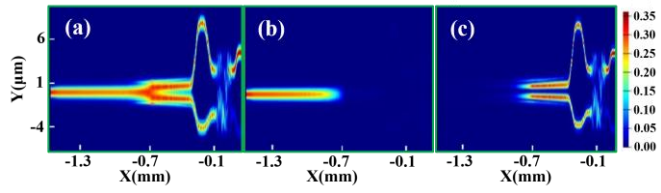

Fig. 3. (a) FDTD simulation showing the electric field intensity magnitude across the complete device with TM_{00} input on the left side and TE_{00} output on the right side. (b) the electric field intensity magnitude of TM components of the propagating wave. (c) the electric field intensity magnitude of TE components of the propagating wave.

This article has been accepted for publication in a future issue of this journal, but has not been fully edited. Content may change prior to final publication. Citation information: DOI 10.1109/LPT.2019.2896560, IEEE Photonics Technology Letters

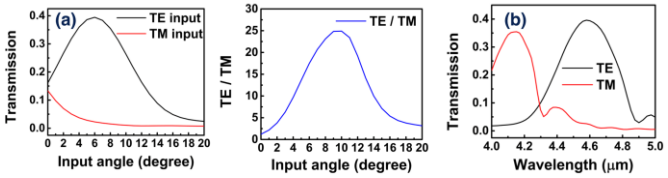

Fig. 4. 2D FDTD simulated transmission for a TE-polarization selective grating coupler versus (a) fiber incident angle and (b) incident wavelength in SoS operating around λ=4.55μm.

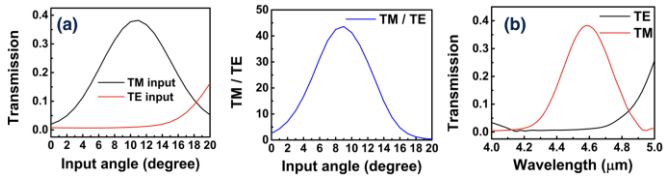

Fig. 5. 2D FDTD simulated transmission for a TM-polarization selective grating coupler versus (a) fiber incident angle and (b) incident wavelength in SoS operating around λ=4.55μm.

(FDTD) simulation results showing the energy transfer from an input TM_{00} to an intermediate TE_{10} and finally output TE_{00} polarization for the designed device, with output TE_{00} in the upper arm 2 only.

Mid-IR optical fibers are not polarization maintaining, hence for effective demonstration of the polarization rotation function at λ~4.55μm, we designed polarization selective grating couplers to efficiently filter the appropriate polarization at the input and output. The parameters of the sub-wavelength structure including air trench width, length, and period, are calculated by using effective index approximation [18].

Figs. 4 and Fig. 5 show FDTD simulation results for the final design of TE and TM polarization selective grating couplers respectively. As can be seen, both are optimized to operate at around λ=4.55μm. Fig. 6 summarizes our optimized design for TE- and TM-polarization selective sub-wavelength grating couplers with 25:1 and 43:1 polarization selectivity respectively at λ=4.55μm for the respective incident angles.

For the polarization rotator design in Fig. 1(a), two devices were fabricated, one with a TM-selective SWG input coupler and the other with a TE-selective SWG input coupler. Both devices had TE-selective grating couplers at both arm1 and arm2 outputs. To account for potential deviations from the desired π/2 phase difference between the two arms of the phase shifter, resulting from fabrication tolerances, we fabricated several devices, with designed phase difference (Δϕ) varying by 0, π/8, π /4, 3 π /8 and π /2 between the two phase shifter arms.

(a)

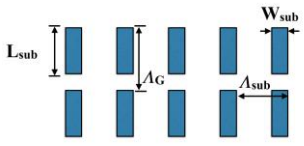

(b)

Parameters	TE Grating	TM Grating
Grating period (Λ_G)	2120 nm	2400 nm
L_{sub}	1272 nm	960 nm
Λ_{sub}	1046 nm	381 nm
W_{sub}	250 nm	250 nm
Angle	8	12
n_{sub}	2.2	2.2

Fig. 6. (a) Schematic illustration of the grating coupler (b) Final design parameters for TE- and TM-polarization selective grating coupler in 900nm thick silicon-on-sapphire. Gratings are broadband.

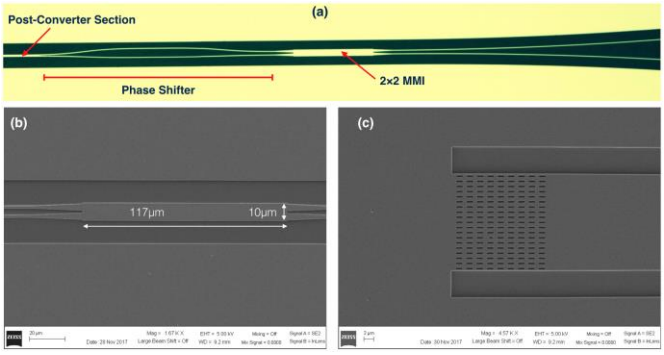

Fig. 7. (a) Microscope image of the polarization rotator. (b) Top view SEM image showing the 2×2 multimode interference power splitter section. (c) Top view SEM image of TE selective grating coupler.

The fabrication process is described in detail in Ref. [19] and is not repeated here. In the final step, the sample is cleaned using Piranha for 15 minutes and followed with three cycles of Piranha/HF post-process treatment. Fig. 7 shows optical and scanning electron microscopy (SEM) images of different sections of the polarization rotator.

III. OPTICAL MEASUREMENT

The details of our experimental setup are described in Ref. [19] with the exception that the light source is substituted with a single special mode quantum cascade laser from Thorlabs, with a center wavelength of 4.55μm and the spectral bandwidth of 130nm.

Prior to the polarization rotator device characterization, propagation losses of single-mode silicon-on-sapphire waveguides were characterized in both polarizations at λ=4.55μm. Single mode ridge waveguide of various lengths were fabricated between the input and output grating couplers. The transmitted power is plotted in Fig 8 normalized to the measured transmittance in the shortest waveguide, and the propagation loss determined by linear fitting. Propagation losses 1.95 dB/cm and 3.06 dB/cm were achieved respectively for 2μm wide single mode TE and TM waveguides. No output power was experimentally observed with SWGs having opposite polarization selectivity at input and output, as expected from simulations in Figs. 4 and 5. We measured a loss ~ 15dB and ~17dB respectively per TE and TM polarization selective grating couplers. The on-chip insertion loss of our polarization rotator device is ~2.5dB.

We measured polarization rotator devices with both TE and TM-polarization filtered inputs. Figs. 9(a) and 9(b) show the TE-polarized power measured in both output arms as a function of the "designed" phase difference (Δϕ) between the two phase-shifter input arms of the 2×2 MMI, for TM-polarized and TE-polarized inputs respectively. In Fig. 9(a), we experimentally measure 80% of the total output power in the upper arm 2 for input TM-polarization for a device with designed Δϕ =3π/8 between the two-phase shifter arms. With TE-input polarization, ~83% of the total output power is measured in the lower arm 1 for the same device, as observed in Fig. 9(b). Since the SWGs in both output arms are TE-polarization selective at the designed incident angle and wavelength, and since we have conservatively chosen a 2mm converter length, it is believed that the reduced power-splitting ratio at the output arms is caused solely by deviations in the fabrication dimensions of the phase shifter component waveguides from design. In order to achieve the highest

This article has been accepted for publication in a future issue of this journal, but has not been fully edited. Content may change prior to final publication. Citation information: DOI 10.1109/LPT.2019.2896560, IEEE Photonics Technology Letters

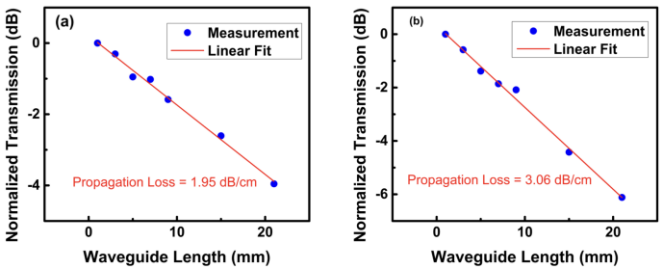

Fig. 8. (a) Propagation loss characteristics of single mode TE strip waveguide in SoS (b) Propagation loss characteristics of single mode TM strip waveguide in SoS

splitting ratio, assuming the same fabrication conditions, Fig. 9 indicates that a design $\Delta\phi$ has to be chosen between $3\pi/8$ and $\pi/2$ in order to achieve the ideal $\Delta\phi=\pi/2$ in fabricated devices. The stringent requirements on the phase shifter also result in a narrow-band device. Thus although >80% conversion efficiency (~1dB loss) from TM_{00} to TE_{10} can be achieved over a much wider wavelength bandwidth, as observed in Fig. 2, our calculations from the experimental data in Fig. 9, indicate that the phase shifter fabrication tolerances limit the total device bandwidth to a narrow band $\Delta\lambda$=125nm centered on λ=4.55μm.

IV. Conclusion

In summary, we have designed and presented a mid-IR silicon-on-sapphire polarization rotator at 4.55μm, to efficiency interface preferential TM-emitting QCLs with preferential TE-guiding slotted PCWs in monolithically integrated mid-IR III-V/ silicon devices for on-chip slow light enhanced optical absorption spectroscopy. The single step etch polarization rotator transfers energy adiabatically from the input TM_{00} mode to an intermediate TE_{10} mode by gradually increasing the width, after which the TE_{10} mode is converted to TE_{00} using a combination of optical phase shifter and 2×2MMIs. Simulations indicate that 100% conversion from TM_{00} to TE_{10} (and thus TE_{00}) can be achieved. Although 80% of the total output power of the device, with TM_{00}-polarized input, is measured in our experiments in the desired output arm 2 at the output with TE_{00} polarization, accurate control of the phase-shifter fabrication will ensure that the remaining 20% of the power that is measured in the other output arm 1 can be added to the desired output arm 2 to achieve 100% of the total output power as TE_{00} in arm 2.

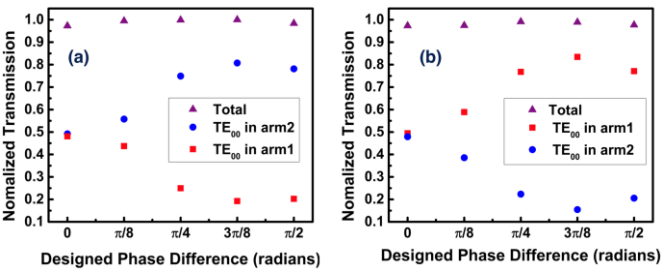

Fig. 9. Normalized Transmission of the two arms and the total (sum of the signal in the two arms) for polarization rotators with a (a)TM-polarization and (b)TE-polarization selective input, and a TE-polarization selective output as a function of the designed phase difference in the upper arm

References

[1] R. Soref, "Mid-infrared photonics in silicon and germanium," *Nature Photonics*, vol. 4, no. 8. pp. 495–497, 01-Aug-2010.

[2] R. A. Soref, S. J. Emelett, and W. R. Buchwald, "Silicon waveguided components for the long-wave infrared region," *J. Opt. A Pure Appl. Opt.*, vol. 8, no. 10, pp. 840–848, Oct. 2006.

[3] L. Labadie and O. Wallner, "Mid-infrared guided optics: a perspective for astronomical instruments," *Opt. Express*, vol. 17, no. 3, pp. 1947–1962, Feb. 2009.

[4] [1] G. C. Holst and S. W. McHugh, "Review of thermal imaging system performance," 1992, vol. 1689, pp. 78–84.

[5] [1] X. Fan and I. M. White, "Optofluidic microsystems for chemical and biological analysis," *Nature Photonics*, vol. 5, no. 10. Nature Publishing Group, pp. 591–597, 18-Oct-2011.

[6] Y. Zou, S. Chakravarty, P. Wray, and R. T. Chen, "Mid-infrared holey and slotted photonic crystal waveguides in silicon-on-sapphire for chemical warfare simulant detection," *Sensors Actuators, B Chem.*, vol. 221, pp. 1094–1103, Dec. 2015.

[7] V. Parro, G. de Diego-Castilla, J. A. Rodríguez-Manfredi, L. A. Rivas, Y. Blanco-López, E. Sebastián, J. Romeral, C. Compostizo, P. L. Herrero, A. García-Marín, M. Moreno-Paz, M. García-Villadangos, P. Cruz-Gil, V. Peinado, J. Martín-Soler, J. Pérez-Mercader, and J. Gómez-Elvira, "SOLID3: A Multiplex Antibody Microarray-Based Optical Sensor Instrument for In Situ Life Detection in Planetary Exploration," *Astrobiology*, vol. 11, no. 1, pp. 15–28, Jan. 2011.

[8] A. Rostamian, J. Guo, S. Chakravarty, C.-J. Chung, D. Nguyen, R. T. Chen, and R. T. Chen, "Parts-Per-Billion Carbon Monoxide Sensing in Silicon-on-Sapphire Mid-Infrared Photonic Crystal Waveguides," in *Conference on Lasers and Electro-Optics*, 2018, p. ATh1O.4.

[9] W.-C. Lai, S. Chakravarty, Y. Zou, and R. T. Chen, "Multiplexed detection of xylene and trichloroethylene in water by photonic crystal absorption spectroscopy," *Opt. Lett.*, vol. 38, no. 19, p. 3799, Oct. 2013.

[10] W. C. Lai, S. Chakravarty, X. Wang, C. Lin, and R. T. Chen, "Photonic crystal slot waveguide absorption spectrometer for on-chip near-infrared spectroscopy of xylene in water," *Appl. Phys. Lett.*, vol. 98, no. 2, p. 023304, Jan. 2011.

[11] A. Lyakh, C. Pflügl, L. Diehl, Q. J. Wang, F. Capasso, X. J. Wang, J. Y. Fan, T. Tanbun-Ek, R. Maulini, A. Tsekoun, R. Go, and C. K. N. Patel, "1.6 W high wall plug efficiency, continuous-wave room temperature quantum cascade laser emitting at 4.6 μm," *Appl. Phys. Lett.*, vol. 92, no. 11, p. 111110, Mar. 2008.

[12] D. Dai and H. Wu, "Realization of a compact polarization splitter-rotator on silicon," *Opt. Lett.*, vol. 41, no. 10, p. 2346, May 2016.

[13] Y. Ding, H. Ou, and C. Peucheret, "Wideband polarization splitter and rotator with large fabrication tolerance and simple fabrication process," *Opt. Lett.*, vol. 38, no. 8, p. 1227, Apr. 2013.

[14] J. Zhang, T.-Y. Liow, M. Yu, G.-Q. Lo, and D.-L. Kwong, "Silicon waveguide based TE mode converter.," *Opt. Express*, vol. 18, no. 24, pp. 25264–70, Nov. 2010.

[15] T. Hu, M. S. Rouifed, H. Qiu, X. Guo, C. G. Littlejohns, C. Liu, and H. Wang, "A Polarization Splitter and Rotator Based on a Partially Etched Grating-Assisted Coupler," *IEEE Photonics Technol. Lett.*, vol. 28, no. 8, pp. 911–914, Apr. 2016.

[16] J. Guo, A. Rostamian, S. Chakravarty, H. Yan, C.-J. Chung, E. Heidari, R. Chen, and R. Chen, "Mid-Infrared Silicon-on-Sapphire Polarization Rotator," in *Conference on Lasers and Electro-Optics*, 2018, p. SF3J.6.

[17] F. Li, S. D. Jackson, C. Grillet, E. Magi, D. Hudson, S. J. Madden, Y. Moghe, C. O'Brien, A. Read, S. G. Duvall, P. Atanackovic, B. J. Eggleton, and D. J. Moss, "Low propagation loss silicon-on-sapphire waveguides for the mid-infrared," *Opt. Express*, vol. 19, no. 16, p. 15212, Aug. 2011.

[18] X. Xu, H. Subbaraman, J. Covey, D. Kwong, A. Hosseini, and R. T. Chen, "Complementary metal-oxide-semiconductor compatible high efficiency subwavelength grating couplers for silicon integrated photonics," *Appl. Phys. Lett.*, vol. 101, no. 3, p. 031109, Jul. 2012.

[19] Y. Zou, H. Subbaraman, S. Chakravarty, X. Xu, and A. Hosseini, "Grating-coupled silicon-on-sapphire integrated slot waveguides operating at mid-infrared wavelengths," *Opt. Lett.*, vol. 39, no. 10, pp. 3070–3073, May 2014.